Influence of a Captured Solvent Molecule on the Isomerization Rates of Calixarenes

T. V. Tolpekina, W. K. den Otter,* and W. J. Briels

Computational Dispersion Rheology, Department of Science and Technology, University of Twente, P.O. Box 217, 7500 AE Enschede, The Netherlands

Received: July 18, 2003; In Final Form: September 26, 2003

The conformational inversion rates of calix[4]arene and *p-tert*-butyl-calix[4]arene in a vacuum and in chloroform have been calculated by using molecular dynamics simulations, as a model study for a process with a pronounced solvent effect. The reaction of *p-tert*-butyl-calix[4]arene in chloroform is complicated by the ability of one of its conformations to capture a chloroform molecule in its cavity, while the smaller cavity of the calix[4]arene is too small for an inclusion. The relatively easily obtained free energies of conformational inversion in a vacuum prove to be a great asset in the calculations with calix[4]arene in chloroform. But they are of limited use for *p-tert*-butyl-calix[4]arene in chloroform, where we had to resort to more advanced methods, to wit, window sampling and a combined coupling parameter−umbrella sampling approach. Conformational inversion rates calculated by the reactive flux method are in good agreement with experimental data.

I. Introduction

Calix[4]arenes are macrocyclic molecules consisting of four phenol rings connected via methylene bridges in the ortho positions with respect to the hydroxyl group, see Figure 1. Ever since their discovery in the 1940s and 1950s, they have continued to attract the attention of supra molecular chemists.[1] Calixarenes are renowned for their usage as building blocks in large aggregates stabilized by hydrogen bonds. Zinke[2] and subsequent workers with calixarenes have noted their propensity to form molecular complexes with smaller molecules, a direct consequence of the presence of a cavity in the center of a calixarene.[3−5] The properties that make calixarenes so popular, their small size and versatility, also make them very suitable for computer modeling. By studying the isomerization process of solvated calixarenes, we want to illustrate and validate the capabilities of current simulation methods.

Calix[4]arenes have four different conformations, distinguished by the rotation of the phenol rings with respect to the central annulus, with the methylene groups acting as hinges. In the "cone" conformation all phenol rings are oriented in the same direction. When one of the phenol rings is rotated with respect to the other three phenol rings, the conformation is called "paco" (short for partial cone). The conformations with two rotated phenol rings are "1,2-alternate" (two neighboring phenol rings have rotated) and "1,3-alternate" (two opposite phenol rings have rotated).

The isomerization reaction from cone to paco will be studied in this article by molecular dynamics simulations (MD). The free energy barrier between these two conformations was determined by NMR experiments to be about 15−16 kcal/mol.[6,7] This means that the molecule stays in the cone conformation for most of the time, and crosses the transition state corresponding to the top of the energy barrier only once every 10 to 100 ms. So, the conformational inversion rate cannot be obtained from a normal MD run, which typically covers only 10 to 100 ns. Previous calculations of rate constants and reaction equilibria have therefore focused on locating the energy minima and transition states, and their normal modes in a vacuum.[8−13]

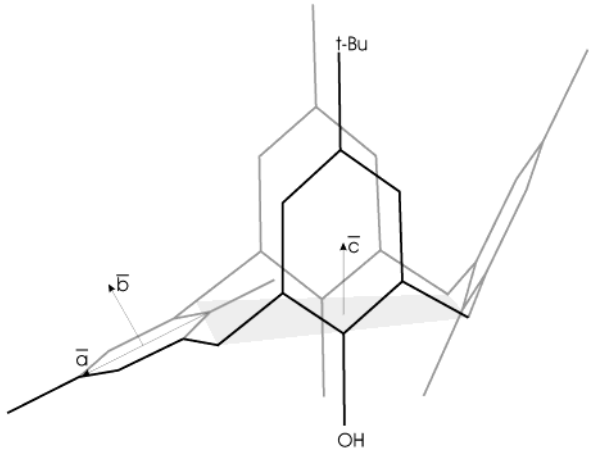

Figure 1. The standard calix[4]arene has hydroxyl groups attached at the lower rim of the benzene rings, and hydrogens at the upper rim. The *p-tert*-butyl-calix[4]arene has $C(CH_3)_3$ groups at the upper rim. The drawn vectors are instrumental in the definition of the reaction coordinate. For clarity, we show the side groups for one phenol ring.

Simulations with solvents have placed the emphasis on the complexation with ions.[14−16] To bridge the aforementioned time gap, in the reactive flux method the reaction rate is expressed as the product of two terms. First the probability of a calix in the cone conformation to reach the top of the energy barrier is calculated. Being an equilibrium property, statistical mechanics offers routes to calculate this probability in the allotted time. Second, the chance that a molecule at the top proceeds to the paco conformation is calculated. These downhill runs proceed very quickly, typically taking only a couple of picoseconds.

For reactions with a clear-cut reaction barrier the above approach works satisfactorily, but less obvious reaction paths require more advanced calculation methods, like "transition path sampling".[17] Although these techniques are well-established, their practical application is frequently less straightforward. Figure 2 shows the radial distribution function of chloroform solvent molecules around a *p-tert*-butyl-calix[4]arene, a calix with *tert*-butyl groups at the upper rim. One clearly sees a sharp

10.1021/jp036100j CCC: $25.00
Published on Web 12/02/2003

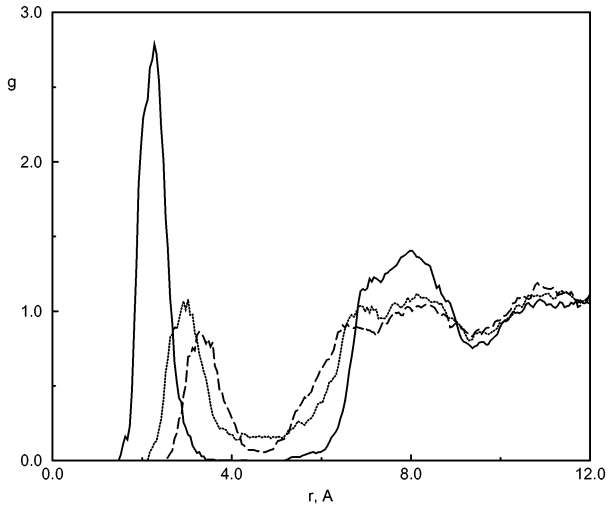

Figure 2. Radial distribution functions of the carbon atom of chloroform relative to the center of mass of the *p-tert*-butyl-calix[4]-arene for the cone (solid line), paco (dashed line), and transition state (dotted line) configuration.

peak followed by a region of zero probability for the cone conformation, indicating that one chloroform molecule is firmly captured in the cavity of the *p-tert*-butyl-calix[4]arene. Inclusions of chloroform, and a range of other molecules, in calix[4]arenes have also been observed by X-ray structure determination,[5,18] NMR,[18,19] and quantum mechanical calculations.[20−22] It suggests that the solvent will have a pronounced effect on the reaction, which complicates the calculations. In Sections II and IV we describe and compare different approaches to this problem. In Section V we find a good agreement between our calculated rates and experimental values, and for the simpler "bare" calix we recover rates previously calculated by a different technique. A detailed analysis of the captured chloroform, and its influence on the reaction, is presented in Section VI.

II. Theory

A. Reaction Rates. The calculation of the reaction rate requires the introduction of a parameter that separates products and reactants. This parameter, or reaction coordinate, ξ, is usually chosen to be a function of the coordinates of the reacting molecule only.[23−25] A reaction coordinate is defined such that it is larger than $\xi^{\neq}$ for products and smaller than $\xi^{\neq}$ for reactants. So, reactants and products are divided by the transition state plane $\xi = \xi^{\neq}$, which is located in the thinly populated area near the top of the energy barrier.

According to Eyring's transition state theory (TST), the forward rate constant is calculated as the instantaneous product-bound flux through the transition state, normalized by the population of the reactant space:[23−28]

$$k_{\mathrm{f}}^{\mathrm{TST}} = \frac{\langle \dot{\xi}\Theta(\dot{\xi})\delta(\xi - \xi^{\neq})\rangle}{\langle \Theta(\xi^{\neq} - \xi)\rangle} = \frac{\langle|\dot{\xi}|\rangle_{\xi^{\neq}}}{2} \frac{P(\xi^{\neq})}{\int_{-\infty}^{\xi^{\neq}} P(\xi)\,\mathrm{d}\xi} \tag{1}$$

Here $\dot{\xi} = \mathrm{d}\xi/\mathrm{d}t$, δ and Θ are the Dirac delta function and Heaviside unit step function, respectively, and the broken brackets denote a canonical average, with the subscript $\xi^{\neq}$ indicating a restriction to the transition state. The probability distribution on the right-hand side represents an integral of the Boltzmann factor over all configurations with the same value of the reaction coordinate:[26,27]

$$P(\xi^*) = \frac{1}{Q}h^{-3N}\int\int \delta[\xi(\mathbf{X}) - \xi^*]\exp[-\beta H(\mathbf{X},\boldsymbol{p}_{\mathbf{X}})]\,\mathrm{d}\mathbf{X}\,\mathrm{d}\boldsymbol{p}_{\mathbf{X}} \tag{2}$$

where H is the Hamiltonian, $\mathbf{X}$ is the collection of all $3N$ coordinates, $\boldsymbol{p}_{\mathbf{X}}$ are conjugate momenta, h is Planck's constant, and $\beta = 1/k_{\mathrm{B}}T$. The partition function Q arises as the normalization factor of the distribution.

Transition state theory gives an over-estimated value as compared with the true reaction rate, because TST does not take into account the possibility of rapid re-crossings.[23−28] For example, a molecule can cross the transition state, collide with a solvent particle, and bounce back to its original configuration. Such a trajectory will contribute to the TST rate (it once crosses the transition state with a positive velocity), but it does not contribute to the true reaction rate. Likewise, re-crossings will also be occurring if the chosen transition state happened to lie below the top of the energy barrier. As a compensation, the reactive flux method (RF) introduces a transmission coefficient κ, whose value lies between 0 and 1:[23,24]

$$k_{\mathrm{f}}^{\mathrm{RF}} = \kappa k_{\mathrm{f}}^{\mathrm{TST}} \tag{3}$$

Under the conditions that classical mechanics adequately describes the motion of the molecule, the transmission coefficient can be calculated exactly. From Onsager's regression hypothesis it follows[23,24] that re-crossings within a time t following the initial crossing reduce the reaction rate by a factor

$$\kappa(t) = \frac{\langle \delta[\xi(0) - \xi^{\neq}]\dot{\xi}(0)\,\theta[\xi(t) - \xi^{\neq}]\rangle}{\langle \delta[\xi(0) - \xi^{\neq}]\dot{\xi}(0)\,\theta[\dot{\xi}(0)]\rangle} \tag{4}$$

If the energy barrier is high, and the energy transfer to the solvent is efficient, then only molecules that are still near the transition state are capable of re-crossing. Once the molecule has reached the reactant or product state, and its excess energy has been dissipated by the solvent, it will only re-cross on a time scale associated with the reaction rate itself. This suggests that $\kappa(t)$ shows a rapid transient decay from a value of 1 to a plateau value, which in turn is decaying very slowly. It is this plateau value that enters in eq 3.

Substituting eq 1 into eq 3, and converting probability distributions into free energies using

$$A(\xi) = -\,k_{\mathrm{B}}T \ln P(\xi) + \text{constant} \tag{5}$$

we rewrite the expression for the RF rate as

$$k_{\mathrm{f}}^{\mathrm{RF}} = \kappa \sqrt{\frac{k_{\mathrm{B}}T}{2\pi}}\left\langle \sqrt{\sum_i \frac{1}{m_i}\left(\frac{\partial \xi}{\partial x_i}\right)^2}\right\rangle_{\xi^{\neq}} \exp\left[-\frac{A(\xi^{\neq}) - A_{\mathrm{R}}}{k_{\mathrm{B}}T}\right] \tag{6}$$

Here A_{R} is the free energy of the integrated probability of the reactant well, and the average velocity of the reaction coordinate has been re-cast in an easily evaluated form.[27,29] In the experimental literature a slightly different definition of the free energy is commonly used, by writing a measured reaction rate as

$$k_{\mathrm{f}}^{\mathrm{exp}} = \frac{k_{\mathrm{B}}T}{h}\exp\left[-\frac{\Delta A^{\neq}}{k_{\mathrm{B}}T}\right] \tag{7}$$

B. Umbrella Sampling. As mentioned in the Introduction, the high free energy barrier means that the molecule stays in one conformation for a long time. The barrier region will be

sampled very poorly in a simulation, and it is quite likely that it is not sampled at all. To eliminate the difficulties with the sampling, we add to the existing potential energy an "umbrella" potential $U(\mathbf{X})$, which reduces the free energy differences between reactants, products, and transition state. The probability distribution of the system with the umbrella potential reads

$$P_U(\xi) = \frac{1}{Q_U} h^{-3N} \int\int \delta[\xi(\mathbf{X}) - \xi^*] \exp[-\beta\{H(\mathbf{X},\boldsymbol{p}_\mathbf{X}) + U(\mathbf{X})\}] \, d\mathbf{X} \, d\boldsymbol{p}_\mathbf{X} \quad (8)$$

In case the umbrella potential is a function of the reaction coordinate only, the distribution in the biased run is easily converted into the probability distribution of the unbiased run,

$$P(\xi) = cP_U(\xi) \exp[\beta U(\xi)] \quad (9)$$

where c is a proportionality constant. The particular choice $U(\xi) = -A(\xi)$ would make P_U a constant, independent of ξ. In the biased run then, the barrier between products and reactants has effectively vanished, and both regions can be sampled sufficiently with a single run. But, at the start of our simulations we do not know what the free energy function looks like, so we can only make educated guesses for the umbrella. If a long simulation with a trial umbrella samples the entire range of the reaction coordinate but the distribution is not reasonably flat, then the sampled probability distribution may be converted into a potential according to eq 5 and added to the existing umbrella to define a new trial umbrella for a second simulation and so on. A useful first guess for an umbrella is the minimum energy as a function of the reaction coordinate.

It all becomes a bit more complicated if the initial guess fails to sample the entire relevant range of the reaction coordinate. In this work we used two extensions of umbrella sampling to circumvent this deficiency. In "windows" sampling[30] the single umbrella for the entire range is replaced by a series of L umbrellas $U_l(\xi)$, $l = 1, ..., L$, each covering a small range of the reaction coordinate. The calculated distributions $P_l(\xi)$ are then combined into a single distribution by using the proportionality constants c to match the partial distributions at the overlap of successive windows. In the second method we combine umbrella sampling with the coupling parameter approach. The later is frequently used for thermodynamic integration of the free energy difference between similar molecules.[31−33] A coupling parameter λ transforms the force field representative of molecule A ($\lambda = 0$) into the force field representative of molecule B ($\lambda = 1$) via a series of intermediate, nonphysical molecules:

$$\Phi(\mathbf{X},\lambda) = (1 - \lambda)\, \Phi_A(\mathbf{X}) + \lambda\, \Phi_B(\mathbf{X}) \quad (10)$$

In the current case, the coupling parameter was used to turn on the interaction between the isomerizing solute and the solvent. We used a series of runs from $\lambda = 1$ (no interaction) to $\lambda = 0$ (full interaction) with $\lambda_{i+1} = \lambda_i - \Delta\lambda$, and a different umbrella potential$U_\lambda(\xi)$ for each λ_i. The probability distribution in this case is just

$$P_\lambda(\xi) = \frac{1}{Q_{U,\lambda}} \int \delta[\xi(\mathbf{X}) - \xi^{\neq}] \exp[-\beta\{\Phi(\mathbf{X},\lambda) + U_\lambda(\xi)\}] \, d\mathbf{X} \quad (11)$$

Like standard umbrella sampling, this will only work efficiently if we have a reasonably flat distribution for each λ_i. This is achieved by using the umbrella that flattened the distribution at λ_i as the first trial umbrella potential for λ_{i+1}, provided the steps $\Delta\lambda$ are sufficiently small.

III. Model and Simulation Details

As a reaction coordinate we use the intuitively appealing angle between the rotating phenol ring and the central annulus. For this purpose, the carbon atoms of the phenol ring are numbered 1 through 6, starting at the carbon connected to the hydroxyl group, and the carbons of the methyl groups connecting rings are labeled a through d, with a and b at either side of the rotating ring. The orientation of the phenol ring is then described by the vectors $\mathbf{a} = \mathbf{x_4} - \mathbf{x_1}$ and $\mathbf{b} = (\mathbf{x_5} - \mathbf{x_2}) \times (\mathbf{x_6} - \mathbf{x_3})$. For the central annulus the vector $\mathbf{c} = (\mathbf{x_a} - \mathbf{x_c}) \times (\mathbf{x_b} - \mathbf{x_d})$ is used. The main value of the reaction coordinate is given by the angle φ_a between **a** and **c**. As this angle proves unreliable for configurations where **a** and **c** are roughly parallel, and to extend the range beyond 0−180°, we introduce a second angle, φ_b, between **b** and **c**. By simple arithmetic manipulations the value of φ_b is made to correspond with φ_a, and a smooth switching function is introduced to combine the two into a single differentiable reaction coordinate.

Both calixarenes were modeled by using the CHARMM parameter set, version 22. This force field has successfully been used for reaction rate calculations and molecular modeling of calixarenes.[12,13,27,29,34] Of course, the results depend on the force field used. The complete force field can be found in ref 12. All bond lengths involving a hydrogen atom were constrained by using the SHAKE algorithm, to accelerate the calculations with a negligible loss of accuracy.[34] For the simulations in a vacuum the range of the nonbonded interactions was set at infinity. In chloroform the intermolecular interactions were truncated at 1.3 nm, using a charge group list, while the nonbonded intra-calix interactions were not truncated at all. The chloroform was modeled as rigid bodies by using the potential of ref 35. The truncated octahedral periodic simulation box contained 317 chloroform molecules surrounding the calix (box size ≈4.4 nm) and 386 molecules around the *p-tert*-butyl-calix[4]arene (≈4.8 nm), which is sufficiently large to prevent any solvent molecule from interacting with a solute and one of its periodic images simultaneously. The temperature and pressure were stabilized at 300 K and 1 bar, by a Nosé-Hoover baro-thermostat, using time constants of 0.1 and 0.5 ps, respectively. All simulations were done with a modified version of DL_POLY_2.0.

IV. Free Energy

As a first estimate for the umbrella we used the minimum energy as a function of the reaction coordinate for the molecule in a vacuum. The minima were calculated by cooling the molecule down to 10 K, with a Gaussian temperature constraint, keeping the reaction coordinate constrained during every run. In the subsequent umbrella runs in a vacuum the region of motion of the reaction coordinate was restricted from −20° to 200°, to reduce the chances of "spontaneous" conformational transitions due to the high stress in the molecule beyond these extremes. These outermost conformations have much higher energies than the cone and paco minima (at approximately 31° and 168°, respectively), thus only highly improbable conformations are excluded. This limitation was done by adding two Fermi−Dirac-like functions to the umbrella, chosen such that they were virtually zero in the interesting region and rapidly increased at the borders. The umbrella potential lowered not only the cone to paco transition state but also the paco to 1,2-alternate and paco to 1,3-alternate transition states. (In the 1,2-alternate conformation, either one of the phenol rings neigh-

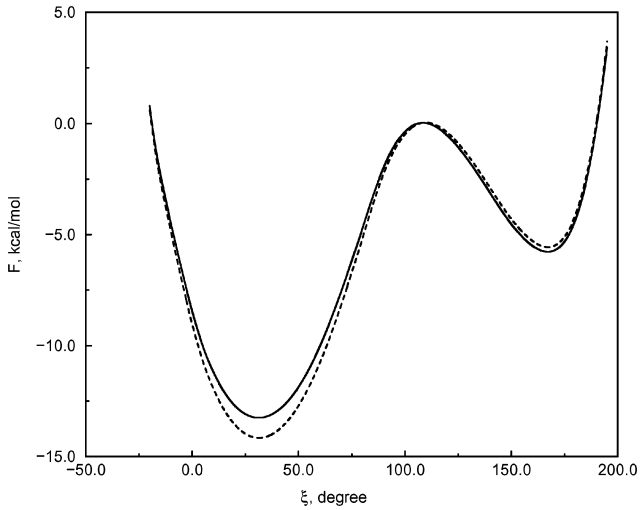

Figure 3. Free energy of a calix[4]arene in a vacuum (solid) and in chloroform (dashed).

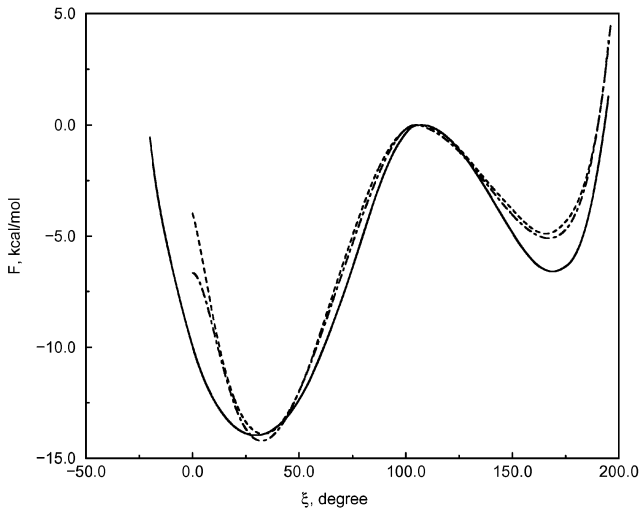

Figure 4. Free energy of a *p-tert*-butyl-calix[4]arene in a vacuum (solid) and in chloroform, obtained with windows umbrella sampling (dashed) and combined coupling parameter−umbrella sampling (dot−dashed).

boring the rotated phenol of the paco is also rotated. In the 1,3-alternate conformation the opposite phenol ring is rotated.) Once a molecule reaches these alternate conformations in a simulation, it does not easily return to the cone or paco conformation. To avoid these problems, the umbrella potential was modified to

$$U(\mathbf{X}) = f(\xi) + f_2(\xi_2) + f_3(\xi_3) + f_4(\xi_4) \qquad (12)$$

where $f(\xi)$ is the initial umbrella potential, and the three $f_i(\xi_i)$ ($i = 2, 4$) are Fermi−Dirac-like potentials depending on the angle between the annular plane and the phenol ring of the respective alternate reaction. Equations 8 and 9 were rewritten accordingly.

The probability distributions in a vacuum obtained with the minimum energy as umbrella were far from flat. For the *p-tert*-butyl-calix[4]arene we even had to use three windows to sample the whole range of ξ. The overall distributions were transformed into extra umbrella potentials according to eq 5, and the systems were run again. This procedure was iterated both for the calix and the *p-tert*-butyl-calix[4]arene. The final simulations, with just one window covering all values of ξ, were continued for 18 and 19 ns for calix and *p-tert*-butyl-calix[4]arene respectively and gave flat distributions. The resulting free energy differences between transition state and cone well were 13.3 kcal/mol for a calix[4]arene and 13.9 kcal/mol for a *p-tert*-butyl-calix[4]arene, see Figures 3 and 4.

The natural choice for the umbrella potential for the simulation of a calix[4]arene in chloroform was the umbrella potential that gave a flat distribution in a vacuum. The run with this umbrella lasted 16 ns. The distribution was transformed into a potential by eq 5, and added to the existing umbrella. With this new umbrella the distribution was satisfactorily flat over 11 ns. The free energy difference between the transition state and the cone well was calculated to be 14.2 kcal/mol, see Figure 3. The increase of this difference showed the same tendency as in previous works.[27,29] We postpone the discussion of the conformational inversion rates until Section V.

The first simulation of a *p-tert*-butyl-calix[4]arene in chloroform was also made with the final vacuum umbrella. This simulation was disastrous: it failed to satisfactorily sample the entire range of the reaction coordinate. The simple reason was that one of the chloroform molecules was caught in the cavity. As mentioned above, we resorted to two different methods to obtain the probability distribution of a *p-tert*-butyl-calix[4]arene in chloroform. In the window sampling approach the vacuum umbrella was used again as a first estimate, supplemented with 10 different windowing potentials, which restricted the motion of ξ roughly to the range from $20°l-40°$ to $20°l$, with l being the number of the window. Because of the narrowness of the windows, the reaction coordinate sampled the whole width, be it with large variations within several of the $P_l(\xi)$. The large overlaps between neighboring windows were exploited to combine the 10 individual distributions into a single overall distribution, which was then transformed into a new umbrella potential for the entire range of ξ. The ensuing distribution was not completely flat, and one more iteration step was taken. The final flat distribution was received by averaging over three runs with different start configurations, each run lasting 9.5 ns. The free energy difference between the transition plane and the cone state is 13.9 kcal/mol, see Figure 4. This value was reproduced by the three individual runs to within 0.1 kcal/mol. We want to draw attention to the shift of the cone, transition, and paco states with respect to their positions in a vacuum.

The second approach was to little by little turn on the interactions between the *p-tert*-butyl-calix[4]arene and the chloroform, while adjusting the umbrella potential at the same time to keep the distribution as flat as possible. We started from the situation $\lambda = 1$, denoting a complete lack of interactions between the *p-tert*-butyl-calix[4]arene and the solvent (but with full-blown interactions within the *p-tert*-butyl-calix[4]arene and within the chloroform). In this case the vacuum umbrella gave a flat distribution, of course. The value of λ was then decreased with steps of $\Delta\lambda = 0.1$. To accommodate the calix, a cavity had to be formed in the chloroform, which was facilitated by the volume rescaling routine used to keep the system at a constant pressure. We used two different systems for the simulations from $\lambda = 0.9$ to 0.3. When the distributions of both systems were found to agree with one another and did not change any more, the average distribution was transformed into the extra umbrella potential to be used for the next λ. The average time for each simulation was 7.5 ns. The simulations from $\lambda = 0.2$ to 0.0 followed the same procedure, with a third system added to increase the precision of the calculations, which were becoming slower because of the increased solvent interactions. The final flat distribution for $\lambda = 0$ was received from three runs with a duration of 9.5 ns each. The free energy difference between the transition plane and the cone state is

TABLE 1: Computed and Experimental Rates of Calix[4]arene in Vacuum and in Chloroform

solvent	k^{TST}, s^{-1}	κ	k^{RF}, s^{-1}	k^{exp}, s^{-1}
vacuum[a]	481	0.42	202	
vacuum[b]	241	0.92	222	
chloroform[a]	110	0.20	22	8,[c] 30[d]
chloroform[b]	84	0.43	36	8,[c] 30[d]

[a] This work. [b] Calculations by den Otter and Briels.[27] [c] Experimental results by Araki et al.[7] [d] Experimental results by Gutsche and Bauer.[6]

TABLE 2: Computed and Experimental Rates of *p-tert*-Butyl-calix[4]arene in Vacuum and in Chloroform

solvent	k^{TST}, s^{-1}	k	k^{RF}, s^{-1}	k^{exp}, s^{-1}
vacuum[a]	151	0.26	39	
chloroform, windows sampling[a]	234	0.09	20	3.6,[b] 12[c]
chloroform, λ sampling[a]	151	0.09	13	3.6,[b] 12[c]

[a] This work. [b] Experimental results by Araki et al.[7] [c] Experimental results by Gutsche and Bauer.[6]

14.2 kcal/mol (see Figure 4). This value compares well with the 13.9 kcal/mol obtained by window umbrella sampling.

V. Conformational Inversion Rate

In the previous section the free energies of our systems were produced as functions of the reaction coordinate, $A(\xi)$. After the substitution of $A(\xi)$ in eq 5, the reaction rate k_f^{TST} is easily calculated by eq 1. The results are collected in Tables 1 and 2. Here the transition state, i.e., $\xi^{\neq}$, was defined as the value of ξ for which $A(\xi)$ reached a maximum. From a physical point of view, a value 10° to the left or to the right would have been equally justified, though it would have produced a different (higher) reaction rate, as explained before. To obtain the true reaction rate, we next calculated the transmission coefficient, see eq 4. The first step was to create configurations belonging to the transition plane, which was done by constraining the reaction coordinate to $\xi^{\neq}$ during a simulation. The atomic coordinates were saved every picosecond. Next, 1000 relaxation runs were performed for each molecule to get the transmission function. These were started with the saved coordinates, combined with random velocities drawn from a velocity-weighted Maxwell−Boltzmann distribution.[34] The transmission coefficients reached their plateau values after about 1 ps, as depicted in Figures 5 and 6. The results for the calix[4]arene are shown in Table 1, those for the *p-tert*-butyl-calix[4]arene in Table 2.

In Table 1 we also included the simulation results from ref 27, which were realized under the same conditions and with the identical force field, but with a different reaction coordinate. This difference led to a different free energy function and therefore to the difference between the transition state theory rates. It is noteworthy that, after multiplication by their respective transmission coefficients, the reaction rates k^{RF} are virtually identical.

The conformational inversion rates are also in good agreement with the values obtained from experimental data. Gutsche and Bauer[6] measured a coalescence temperature with temperature-dependent ^{1}H NMR for the hydrogens connected to the hinge carbons, and derived the isomerization rate at this temperature from the chemical shift. They converted the rate into a free energy by

$$\Delta A^{\neq} = RT_{\text{coalescence}} \ln\left(\frac{6.62 \times 10^{12}}{k_{\text{coalescence}}}\right) \qquad (13)$$

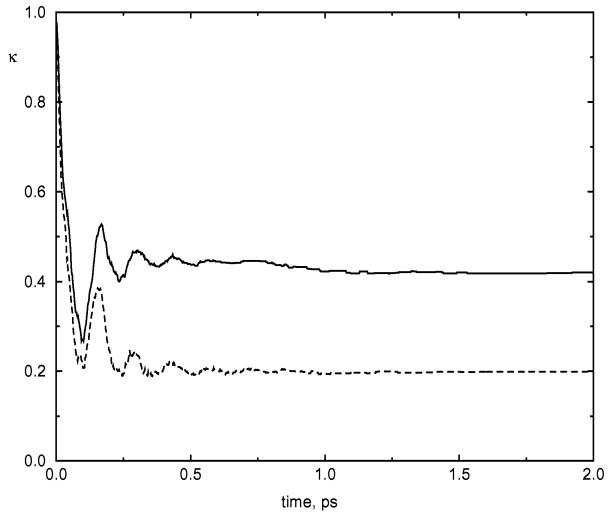

Figure 5. Transmission coefficients of a calix[4]arene in a vacuum (solid) and in chloroform (dashed).

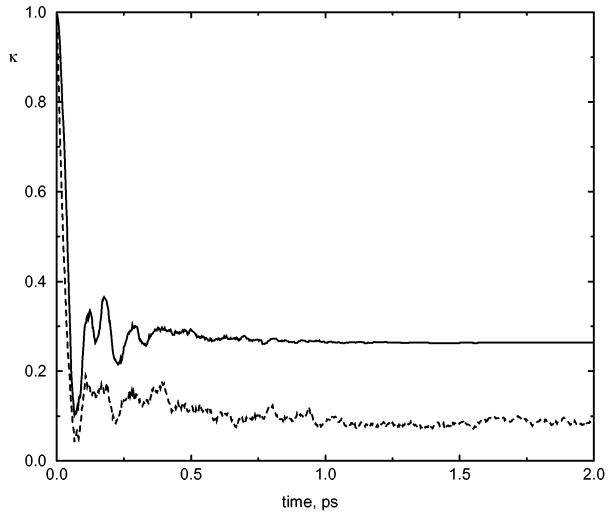

Figure 6. Transmission coefficients of a *p-tert*-butyl-calix[4]arene in a vacuum (solid) and in chloroform (dashed).

Araki et al.[7] measured the reaction rate as a function of temperature and obtained the free energy from an Arrhenius plot. Assuming that the free energy is independent of the temperature, we calculated the reaction rates at 300 K from the data provided in refs 6 and 7 by eq 7. These rates correspond to the cone to inverted cone reaction (all four rings have rotated), because the intermediate conformations have too short a lifetime to be detectable, and are therefore not directly comparable to our rates.

The inversion reaction consists of four steps, with one phenol ring rotating in each step.[12] These steps are independent, as the energy barriers between consecutive minima are much higher than k_BT. In schematic form,

$$\mathrm{C} \underset{k_2}{\overset{k_1}{\rightleftharpoons}} \mathrm{P} \underset{k_4}{\overset{k_3}{\rightleftharpoons}} \mathrm{A} \underset{k_3}{\overset{k_4}{\rightleftharpoons}} \mathrm{P}' \underset{k_1}{\overset{k_2}{\rightleftharpoons}} \mathrm{C}' \qquad (14)$$

where C, P, and A denote the sum of all cone, paco, and alternate conformations, respectively, and where primes indicate conformations in which the majority of the phenol rings are pointing downward. Our calculations concern the rotation of *one* of the phenol rings of a cone. As there are four phenol rings, the overall cone-to-paco rate is four times higher, $k_1 = 4k_f^{RF}$. The calculated free energy functions can also be used to

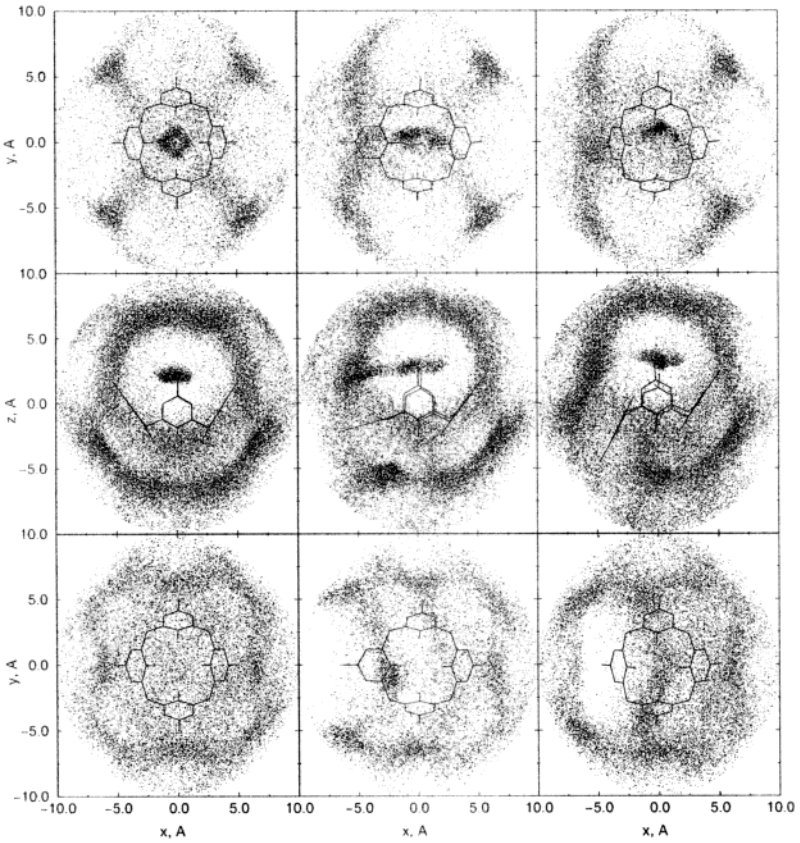

Figure 7. Density distributions of the carbon atoms of chloroform, after correcting for the orientation of the *p-tert*-butyl-calix[4]arene. From left to right are shown the cone, transition state, and paco conformation. The middle row gives a side view, the upper row a top view of the carbons with a positive *z*-coordinate, and the bottom row a top view of the carbons with a negative *z*-coordinate. The configurations shown are averaged over the simulation.

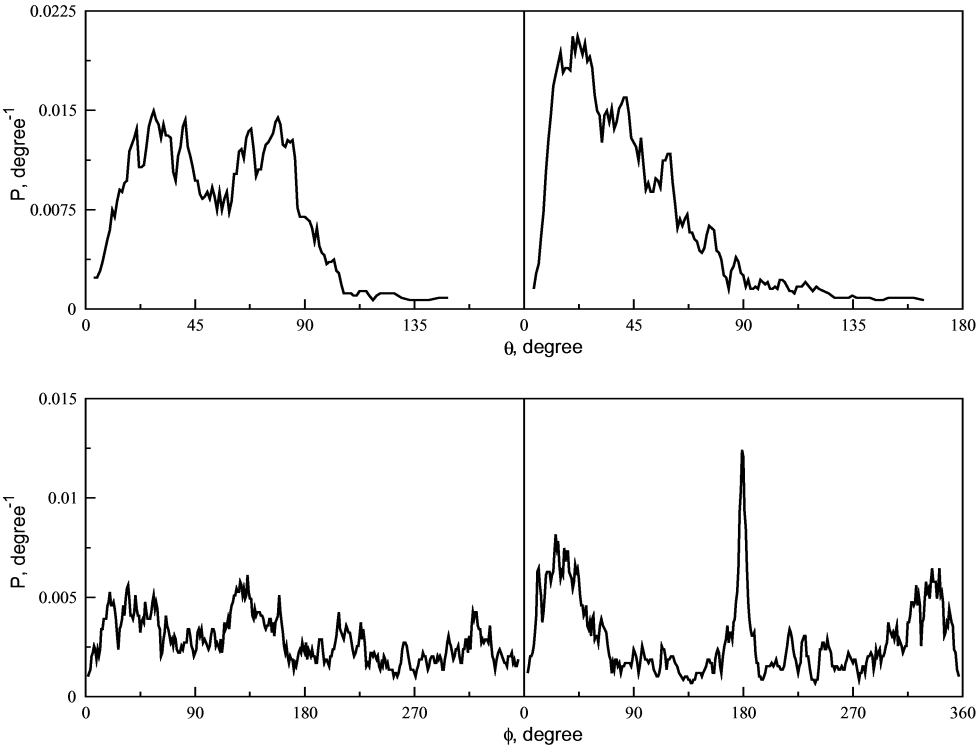

Figure 8. Probability distributions of the angles describing the orientation of the nearest chloroform molecule for the cone (left) and paco (right) conformations. Note that for a perfectly random distribution $P(\theta) \sim \sin(\theta)$ and $P(\phi) =$ constant.

determine the reverse reaction rates, from paco to cone, which have the exact same transmission coefficients as the forward reactions. In this case the ordinal number of the rotating phenol is fixed by the particular paco conformation one is looking at,

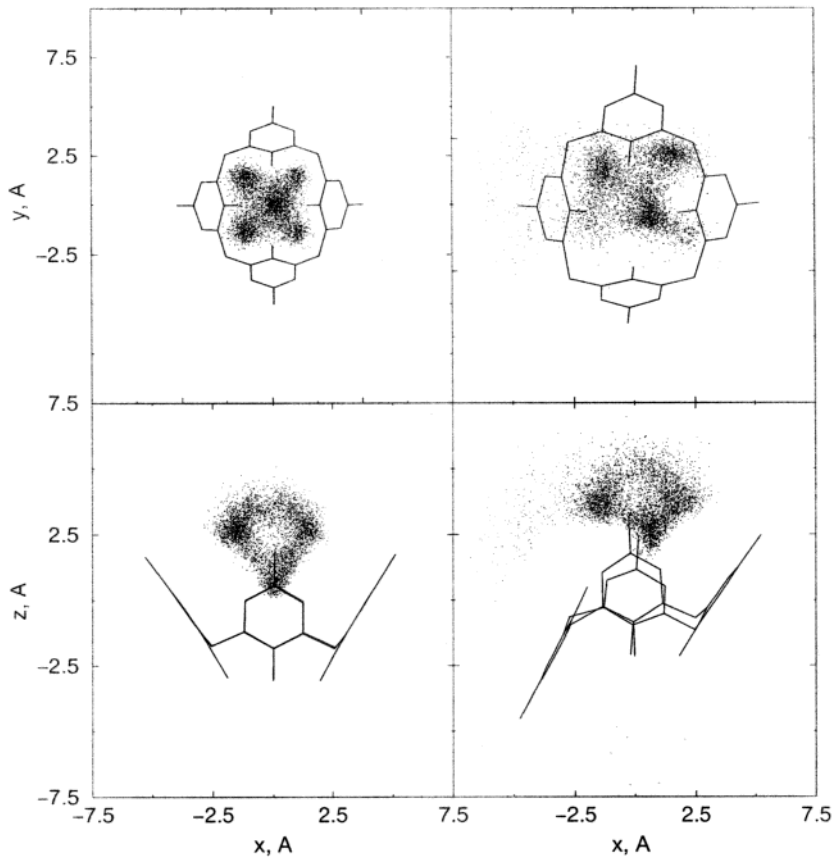

Figure 9. Density distributions of the chlorine atoms of the captured chloroform molecule, in cone (left) and paco (right) conformations. The upper row gives a top view, and the bottom row a side view. The configurations shown are averaged over the simulation.

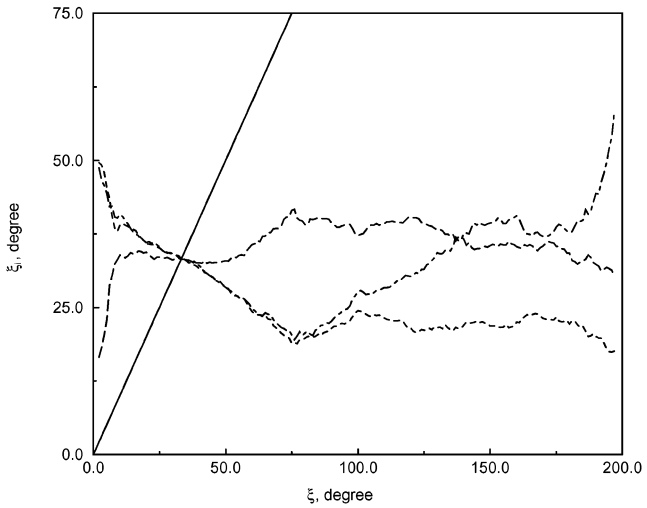

Figure 10. The equilibrium angles of the phenol rings to the right (dot−dashed), to the left (dashed), and opposite (long dashed) to the rotating phenol ring as functions of the reaction coordinate. The straight line denotes the rotating ring itself.

hence $k_2 = k_r^{RF} = 0.97 \times 10^8\ s^{-1}$ for *p-tert*-butyl-calix[4]arene. Any paco can proceed to an alternate conformation through three different routes, by rotating the phenol ring to the left, to the right, or opposite to the rotated phenol ring of the paco. The latter reaction requires breaking up two hydrogen bonds, and the former two reactions require breaking up only one hydrogen bond and are therefore much quicker, $k_3 = k_3' + k_3''$. Because of the directionality of the hydrogen bonds, the rates of the two paco to 1,2-alternate reactions are different. Applying transition state theory to the free energy profile in a vacuum, we find $k_3' = 0.35 \times 10^8\ s^{-1}$ and $k_3'' = 0.69 \times 10^8\ s^{-1}$. Next, the set of

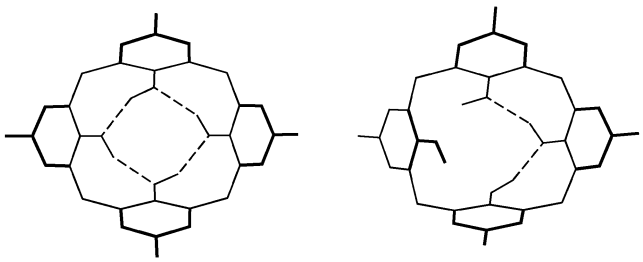

Figure 11. The cone (left) and paco (right) conformations with their hydrogen bonds at the lower rim.

coupled differential equations represented by eq 14 is analytically solved to give five relaxation times, the largest of which corresponds to the inversion process. Inserting the above numerical values (k_4 is irrelevant), the final expression for the *p-tert*-butyl-calix[4]arene reads

$$k_{inv}^{exp} \approx 2k_f^{RF} \tag{15}$$

An identical analysis of the calix, with k_2 though k_3 determined by using the methods outlined above, yields[27,29]

$$k_{inv}^{exp} \approx 3k_f^{RF} \tag{16}$$

By inverting these equations, we arrive at the experimental rates listed in Table 1 and Table 2. They agree very well with our simulation results.

VI. Structural Analysis

The above numerical results show a mixed picture. On one hand, the free energy curve of the calix is nearly identical in a

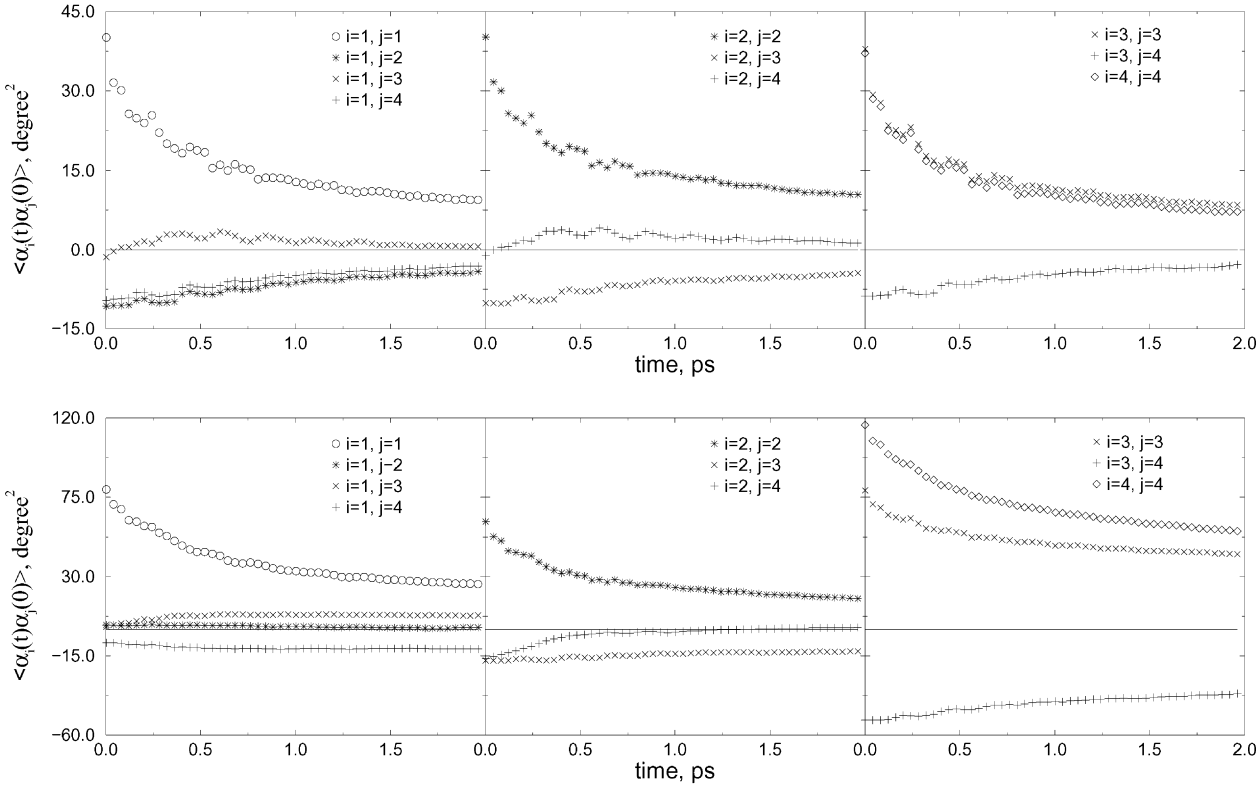

Figure 12. Correlation functions of the angles of phenol rings *i* and *j*, with $\alpha_i = \xi_i - \langle \xi_i \rangle$. The upper row gives the correlation functions for the cone conformation, the lower row those for the paco.

vacuum and in solvent. The small differences and the reduced transmission coefficient do, however, reduce the conformational inversion rate in solvent by nearly an order of magnitude. On the other hand, the free energy profile of the *p-tert*-butyl-calix-[4]arene has drastically changed in the solvent, but the final conformational inversion rate has gone down only by a factor of 2 to 3. It is difficult to determine in which way exactly the interactions between the solute and the solvent, and the induced changes in the entropies and internal energies of the solute and the solvent, affect the reaction.

The interplay between solute and solvent can perhaps be better understood by studying the distribution of the solvent in the first solvation shell around the solute. In Figure 7 scatter plots are given of the positions of the carbon atoms of the chloroform molecules in the vicinity of the *p-tert*-butyl-calix[4]arene. These plots were collected from simulations of about 1 ns each. The simulation of the cone was run with the normal force field, the paco required an extra potential to prevent the rare spontaneous transition to a cone, while the transition state could only be sampled by constraining the reaction coordinate. In the analysis, the translational and rotational displacements of the *p-tert*-butyl-calix[4]arene were calculated and the whole box was subjected to the same correction to keep the *p-tert*-butyl-calix[4]arene at a constant position and orientation, before the relative positions of the chloroforms were determined.[27,34] Comparable plots for the calix[4]arene can be found in ref 27. Although a different reaction coordinate was used in those calculations, there are no discernible differences for the distributions around the transition state of the calix[4]arene. As the simulations of cone and paco do not depend on the reaction coordinate at all, they obviously are identical.

The two top plots in the left column of scatter clearly show that the *p-tert*-butyl-calix[4]arene in the cone configuration captures a chloroform inside its cavity. The radial distribution function of the chloroform around the cone, see Figure 2, reveals a wide gap around 4.5 Å, suggesting that the captured chloroform molecule hardly ever escapes. This is also corroborated by the fact that in all simulations of a cone, one and the same chloroform was observed to reside within the cavity throughout the entire simulation. In the calix, on the other hand, there is a tendency for a chloroform to hover just above the calix, but this chloroform is exchanged regularly (about once every 0.5 ns) for another chloroform. Below both calixarenes, the polar hydroxyl groups are not capable of orienting the polar chloroform. The plots in the middle column and those in the right column show that the transition state and the paco also induce quite some structure in the solvent, but they are not capable of immobilizing a chloroform.

The orientation of the chloroform molecule inside the cavity of the *p-tert*-butyl-calix[4]arene can be described with two angles. The angle θ is defined as the angle between the vector **d**, pointing from a chloroform hydrogen to its carbon, and the normal vector **c** introduced earlier. Figure 8 shows that the vector **d** is pointing downward with two preferred angles of approximately 25° and 75° for the cone conformation. The first maximum corresponds to an orientation with the hydrogen of the chloroform pointing toward the annulus, and the second maximum corresponds to an orientation with one of the chlorines pointing down. In X-ray diffraction experiments on the solid state of a complex of *p-tert*-butyl-calix[4]arene and chloroform, a value of 68° was found for θ at room temperature.[19] This corresponds well with our second peak, though it should be noted that the orientation in the solid state need not be identical with that in the liquid state. In further agreement with their findings, the top left plot in Figure 7 shows that the carbon of the chloroform does not lie above the center of the calix. The second angle is obtained by projecting **d** onto the annular plane of the calix, and calculating the angle, ϕ, between this projection and the coplanar vector $\mathbf{x_b} + \mathbf{x_c} - \mathbf{x_a} - \mathbf{x_d}$. Thus, an angle of 90° indicates that the hydrogen of the chloroform is directed

toward the rotating phenol ring, 180° corresponds with the hydrogen directed at the neighboring phenol to the left (at the top view), and so on. The captured molecule rotates freely inside the cavity of the cone conformer, as can be seen from the distribution of ϕ in Figure 8. Four-fold symmetry relating to the symmetry of the calix is visible, with maximum between the phenol rings. The density distribution of the chlorines of the captured chloroform reveals a similar symmetry, see Figure 9, again with a preference for the positions directly above the hinge carbons. In the paco conformation the rotations of the chloroform are significantly reduced. Its hydrogen is predominantly directed at 25° with respect to the annulus. The in-plane distribution has only three peaks: one on either side of the ring to the left of the rotating ring and one directly at the ring to the right. Figure 9 reveals that there are only three regions of high chlorine density left, all of which lie at the same side of the *p-tert*-butyl-calix[4]arene.

As mentioned before, we introduced an angle for each of the three phenol rings besides the rotating phenol ring. The average values of these four angles are given in Figure 10 as functions of the reaction coordinate. The rotations of the nonreacting phenol rings were limited to a maximum of 85° to avoid reactions to alternate conformations, a value seen here to lie far beyond the typical value of these angles. All lines intersect at 33°, which corresponds to the stable cone conformation. This conformation is symmetric because the four hydroxyl groups at the lower rim form a cyclic array of four hydrogen bonds, see Figure 11. When the phenol ring rotates between 0° and 75°, the angles of its two neighboring rings are identical. But as this ring rotates further, two hydrogen bonds are broken, see Figure 10, and an asymmetric paco conformation is reached with the two neighbors (one a donor, one an acceptor) at different angles, see Figure 11. In a vacuum the disparity between the two rings is already present, with equilibrium values of about 15° and 22°, respectively. The asymmetrical position of the chloroform enlarges this difference.

Auto- and cross-correlation functions of the angles are depicted in Figure 12 for the cone and paco conformations. The standard force field was used, supplemented in the case of the paco with a potential to prevent its transition to the cone conformation. Each run lasted 2 ns, with angles stored every 2 fs. For the cone there are only three distinct correlation functions, as expected from its symmetry. In agreement with Figure 10, the transient correlation between any ring and its two neighboring rings is negative and bigger than that with its opposite ring. The correlations for the paco are all different, due to the lack of symmetry. The fluctuations of the angles are about 40% bigger in this case, as expected with the reduced number of hydrogen bonds. Surprisingly, the auto-correlations of rings 3 and 4 and their cross-correlation are slower than for the cone. From the small amplitudes of all cross-correlations, and the limited shift of the equilibria observed in Figure 10, we conclude that the coupling between two rings is so weak that the isomerization steps in eq 14 are independent.

Further insight into the reaction process is obtained from the average energies of the conformations. In a vacuum, the energy difference between cone and paco is $\Delta E^{\mathrm{vac}} = \langle E^{\mathrm{vac}}_{\mathrm{paco}} \rangle - \langle E^{\mathrm{vac}}_{\mathrm{cone}} \rangle = 9.2$ kcal/mol. This difference is mainly due to Coulombic interactions, which account for 7.8 kcal/mol, and bending terms, 1.4 kcal/mol, with the remaining terms adding less than 0.7 kcal/mol each. The free energy difference between the two conformations is $\Delta A^{\mathrm{vac}} = 7.4$ kcal/mol, implying that the entropy of the paco is higher by $\Delta S^{\mathrm{vac}} = 6$ cal/(mol K). In chloroform the difference in the total energies has risen to $\Delta E^{\mathrm{sol}} = 11.9$ kcal/mol, hence $\Delta\Delta E = 2.7$ kcal/mol. This rise is mainly due to an increase of the van der Waals interactions (including interactions with and within the solvent) by $\Delta\Delta E^{\mathrm{vdw}} = 3.5$ kcal/mol, while the Coulombic and bending terms dropped by 1.0 kcal/mol each. We think that these differences, which stabilize the cone with respect to the paco, arise mainly from the strong binding with the captured chloroform molecule. The solvent increased the free energy difference to $\Delta A^{\mathrm{sol}} = 9.0$ kcal/mol ($\Delta\Delta A = 1.6$ kcal/mol). The entropy difference is therefore even larger in chloroform, $\Delta S^{\mathrm{sol}} = 9.7$ cal/(mol K) ($\Delta\Delta S = 2.7$ cal/(mol K)), which we speculate is largely caused by the immobilization of one chloroform inside the cavity of the *p-tert*-butyl calix[4]arene. Elsewhere we present a comparison of these results with quantum mechanical calculations, using a continuum model to represent the solvent.[36]

VII. Conclusions

The isomerization rates of calix[4]arene and *p-tert*-butyl-calix[4]arene in a vacuum and in chloroform have been studied with molecular dynamics simulations. Whereas the free energy as a function of the angle of the rotating phenol was relatively easily calculated for the former molecule, it proved much harder for the latter as it held on with tenacity to a chloroform molecule. Two methods were tried in the latter case: windows umbrella sampling and a combined coupling parameter−umbrella approach. Both methods coped well with the captured chloroform, their final free energy distributions being very similar, though the combined coupling parameter−umbrella approach required much more time than windows umbrella sampling. The reactive flux method was used to obtain the conformational inversion rate constants. All rates are in good agreement with the experimental data. The conformational inversion rate of the calix[4]arene is close to the value previously calculated with a different reaction coordinate, illustrating the robustness of the reactive flux method.

Acknowledgment. This work is part of the research programs of Chemische Wetenschappen (CW) and of the Stichting voor Fundamenteel Onderzoek der Materie (FOM), which are financially supported by the Nederlandse Organisatie voor Wetenschappelijk Onderzoek (NWO).

References and Notes

(1) Gutsche, C. D.; Rogers, J. S.; Stewart, D.; See, K.-A. *Pure Appl. Chem.* **1990**, *62*, 485.
(2) Zinke, A.; Kretz, R.; Leggewie, E.; Hössinger, K. *Monatsh. Chem.* **1952**, *83*, 1213.
(3) Gutsche, C. D. *Acc. Chem. Res.* **1982**, *16*, 161.
(4) Andreetti, G. D.; Pochini A.; Ungaro R. *J. Chem. Soc., Perkin. Trans. 2* **1983**, 1773.
(5) Ungaro R.; Pochini, A.; Andreetti, G. D.; Sangermano, V. *J. Chem. Soc., Perkin. Trans. 2* **1984**, 1979.
(6) Gutsche, C. D.; Bauer, L. J. *J. Am. Chem. Soc.* **1985**, *107*, 6052.
(7) Araki, K.; Shinkai, S.; Matsuda, T. *Chem. Lett.* **1989**, *1989*, 581.
(8) Harada, T.; Rudzinski, J. M.; Osawa, E.; Shinkai, S. *Tetrahedron* **1993**, *49*, 5941.
(9) Harada, T.; Ohseto, F.; Shinkai, S. *Tetrahedron* **1994**, *50*, 13377.
(10) Grootenhuis, P. D. J.; Kollman, P. A.; Groenen. L. C.; Reinhoudt, D. N.; van Hummel, G. J.; Ugozzole, F.; Andreeti, G. D. *J. Am. Chem. Soc* **1990**, *112*, 4165.
(11) van Hoorn, W. P.; Morshuis, G. H.; van Veggel, F. C. J. M.; Reinhoudt, D. N. *J. Phys. Chem. A* **1998**, *102*, 1130.
(12) Fischer, S.; Grotenhuis, P. D. J.; Groenen, L. C.; van Hoorn, W. P.; van Veggel, F. C. J. M.; Reinhoudt, D. N.; Karplus, M. *J. Am. Chem. Soc.* **1995**, *117*, 1611.
(13) Schlachter, I.; Höweler, U.; Iwanek, W.; Urbaniak, M.; Mattay, J. *Tetrahedron* **1999**, *55* (52), 14931.
(14) Guilbaud, P.; Varnek, A.; Wipff, G. *J. Am. Chem. Soc.* **1993**, *115*, 8298.
(15) Varnek, A.; Wipff, G. *J. Phys. Chem.* **1993**, *97*, 10840.

(16) Abidi, R.; Baker, M. V.; Harrowfield, J. M.; Ho, D. S.-C.; Richmond, W. R.; Skelton, B. W.; White, A. H.; Varnek, A.; Wipff, G. *Inorg. Chim. Acta* **1996**, *246*, 275.

(17) Bolhuis, P. G.; Chandler, D.; Dellago, C.; Geissler, P. L. *Annu. Rev. Phys. Chem.* **2000**, *53*, 291.

(18) Brouwer, E. B.; Enright, G. D.; Ripmeester, J. A. *Supramol. Chem.* **1996**, *7*, 7.

(19) Benevelli, F.; Bond, A.; Duer, M.; Klinowski, J. *Phys. Chem. Chem. Phys.* **2000**, *2*, 3977.

(20) Backes, A. C.; Schatz, J.; Siehl, H.-U. *J. Chem. Soc., Perkin. Trans. 2* **2002**, 484.

(21) Ogden, M. I.; Rohl, A. L.; Gale, J. D. *Chem. Commun.* **2001**, 1626.

(22) Brouyère, E.; Persoons, A.; Brédas *J. Phys. Chem. A* **1997**, *101*, 4142.

(23) Hänggi, P.; Talkner, P.; Borkovec, M. *Rev. Mod. Phys.* **1990**, *62*, 251.

(24) Chandler, D. J. *J. Chem. Phys.* **1978**, *68*, 2959.

(25) Atkins, P. W. *Physical Chemistry*; Oxford University Press: Oxford, UK, 1990; pp 484, 597, and 840.

(26) Frenkel, D.; Smit, B. *Understanding Molecular Simulation*; Academic Press: San Diego, CA, 1996; pp 176 and 249.

(27) den Otter, W. K.; Briels, W. J. *J. Am. Chem. Soc.* **1998**, *120*, 13167.

(28) Eyring, H. J. *J. Chem. Phys.* **1935**, *3*, 107.

(29) den Otter, W. K.; Briels, W. J. *J. Chem. Phys.* **1997**, *107*, 4968.

(30) Kumar, S.; Bouzida, D.; Swedsen, R. H.; Kollman, P. A.; Rosenberg, J. M. *J. Comput. Chem.* **1992**, *13*, 1011.

(31) Zacharias, M.; Straatsma, T. P.; McCammon, J. A. *J. Chem. Phys.* **1994**, *100*, 9025.

(32) Mazor, M. H.; McCammon, J. A.; Lybrand, T. P. *J. Am. Chem. Soc.* **1989**, *111*, 55; **1990**, *112*, 4411.

(33) Pearlman, D. A.; Kollman, P. A. *J. Chem. Phys.* **1991**, *94*, 4532.

(34) den Otter, W. K.; Briels, W. J. *J. Chem. Phys.* **1997**, *106*, 5494.

(35) Dietz, W.; Heizinger, K. *Ber. Bunsen-Ges. Phys. Chem.* **1984**, *88*, 543; **1985**, *89*, 986.

(36) Aleman, C.; den Otter, W. K.; Tolpekina, T. V.; Briels, W. J. Submitted for publication.